EJNMMI Radiopharmacy and Chemistry

RESEARCH ARTICLE Open Access

An ACE2 PET imaging agent derived from ^{18}F/Cl exchange of MLN-4760 under phase transfer catalysis

Pan Zhou[1,2†], Kai Ning[3†], Shuai Xue[2], Qingqing Li[3], Danni Li[1], Haijun Yang[4], Zeying Liang[4], Rou Li[1], Jian Yang[4*], Xiao Li[1,2,5*] and Lan Zhang[2*]

†Pan Zhou and Kai Ning contributed equally to this work.

*Correspondence:
Jian Yang
yj_scu@163.com
Xiao Li
lixiao@sinap.ac.cn
Lan Zhang
zhanglan@sinap.ac.cn
[1]Department of Nuclear Medicine, Shanghai Changhai Hospital, Shanghai 200433, China
[2]Shanghai Institute of Applied Physics, Chinese Academy of Sciences, Shanghai 201800, China
[3]Artery Pharmaceuticals, Shanghai 201413, China
[4]School of Medicine, Shanghai University, Shanghai 200444, China
[5]Shanghai Key Laboratory of Molecular Imaging, Shanghai University of Medicine and Health Sciences, Shanghai 201318, China

Abstract

Background Angiotensin-converting enzyme-2 (ACE2) acts as a key regulatory molecule and important therapeutic target in the pathological remodeling of numerous organs and diseases. In this study, a rapid, simple, and efficient synthetic route with a catalytic, ^{18}F-for-Cl (^{18}F/Cl) exchange scheme was designed for the preparation of ^{18}F-labeled MLN-4760, and its targeting ability was investigated in a humanized ACE2 mouse model.

Results A novel ^{18}F-labeled MLN-4760 radioligand, abbreviated as ^{18}F-MLN-4760, was successfully synthesized by the ^{18}F/Cl exchange-labeling, and was purified by SepPak C18 columns with a radiochemical yield of 30% and a radiochemical purity of 29.89%. Target distribution of ^{18}F-MLN-4760 in several organs with high ACE2 expression was observed by PET imaging with good stability over 120 min. The biodistribution data showed that the uptake of ^{18}F-MLN-4760 in ACE2-overexpressing organs and tissues was highly specific, and immunohistochemistry confirmed the same results of ACE2 expression and biodistribution in the major organs (heart, liver, lungs, and kidneys). There was a good correlation between the uptake in the organs with high ACE2 expression and ACE2 expression levels ($r = 0.935$).

Conclusion ^{18}F-MLN-4760 was successfully synthesized via ^{18}F/Cl exchange under phase transfer catalysis, and served as a potential probe for ACE2-targeted PET imaging.

Keywords MLN–4760, ACE2, ^{18}F/Cl exchange, PET imaging agent, Phase transfer catalysis

Background

Angiotensin-converting enzyme 2 (ACE2) is a key protease in the renin–angiotensin system (RAS) and was the first human ACE homologue (Donoghue et al. 2000). ACE2, a new protein-zinc metalloproteinase, was initially thought to be distributed only in the kidneys, heart, and testes, but was subsequently found to be expressed to varying degrees in the lungs, brain, liver, spleen, pancreas, stomach, intestine, bladder, adipocytes, and vascular endothelial cells (Roca-Ho et al. 2017; Hikmet et al. 2020). ACE2 is

involved in the maintenance of long-term in vivo homeostasis of the RAS for blood pressure, fluids, and electrolytes mainly through the ACE2/angiotensin-(1–7) [Ang-(1–7)]/Mas receptor axis (Fontes et al. 1994; Santos et al. 2018).

ACE2 serves as a key regulator and important therapeutic target in a variety of disease models, such as novel coronavirus infections, cardiovascular diseases, diabetes, hypertension, tumors, and obesity (Xie et al. 2021; Lin et al. 2022; Gheblawi et al. 2020), and the monitoring of dynamic alterations in organ-specific or lesion-specific ACE2 is of great value in probing disease progression and guiding disease treatment protocols. Existing ACE2 clinical detection methods are mainly based on protein immunoblotting, polymerase chain reaction, and enzyme-linked immunosorbent assay for the detection of blood ACE2 levels, or immunohistochemistry and transcriptome sequencing technology for the in vitro analysis of isolated tissues (Widowati et al. 2023; Wei et al. 2023), which is insufficient for the application in diverse types of diseases and complex pathophysiological reconstructive processes. Given that the in vivo visual observation of ACE2 cannot be achieved, it is not possible to evaluate its dynamic changes. Blood levels of ACE2 are unable to elaborate of associations between its dysfunction and organs and systems, and it is difficult to explore the disease process from the molecular level (Yang et al. 2021). Therefore, in vivo spatial distribution and tissue quantification of ACE2 is an unmet need of a breakthrough. Molecular imaging technology uses radioligands to trace disease-associated biomarkers or pathways to accurately provide quantitative spatial distribution of physiologically relevant targets, which holds the promise of visual detection of ACE2 at the in vivo level.

MLN-4760 is a known human ACE2 inhibitor (IC50, 0.44 nm) that is 5000-fold more selective than the related enzymes including human testicular ACE (IC50, >100 μM) and bovine carboxypeptidase A (IC50, 27 μM) (Wang et al. 2024; Joshi et al. 2016). It specifically binds to the ACE2 receptor after the preliminary completion of in vivo distribution, and the amount of binding increases with the increase in the number of ACE2 receptors (Joshi et al. 2016). At present, the biodistribution of MLN-4760 of animals cannot be detected by conventional biochemical means (fluorescence resonance energy transfer, ELISA, etc.) (Dales et al. 2002), so how to conveniently and quickly detect the ACE2-targeting distribution of MLN-4760 in vivo is a problem that needs to be solved. Currently, receptor imaging with ^{18}F-labeled ligand is a major area of molecular nuclear medicine research, and the use of positron emission tomography/computed tomography (PET/CT) provides monitoring data with high sensitivity and resolution (Deng et al. 2019). Among a large number of positron-emitting nuclides, much like Cu-64 and Ga-68 which dominate the field of radiolabelling of peptides, ^{18}F has excellent nuclear and chemical properties, with a small atomic radius, a half-life of 109.8 min, a maximum positron energy of 0.64 MeV, and an average distance of 0.22 mm in tissue-penetration, that is why it suits for ligands labeling and PET imaging (Sahnoun et al. 2020; Cole et al. 2014; Huo 2015). Based on the fact that the 3, 5-positions of the benzene ring of MLN-4760 contains two chlorine atoms, we propose substituting the ^{18}F for Cl (^{18}F/Cl) by the nucleophilic aromatic substitution reaction (SNAr) mechanism, thereby establishing a strategy for targeting ACE2 as a PET imaging agent. In addition, this study evaluated its biodistribution and specificity for targeting ACE2 in a humanized ACE2 mouse model.

Materials and methods

Main instruments

The main equipment used in this study included a 1260 Infinity II high-performance liquid chromatography (HPLC) (Agilent Technologies, Inc., USA), a 6540/6545 Q-TOF liquid chromatography-mass spectrometer (LC-MS) (Agilent Technologies, Inc., USA), a high pressure reactor (Shanghai Titan Technology Co., Ltd, China), a Olympus BX43 inverted fluorescence microscope (Olympus Corporation, Japan), a GC-2101 gamma counter (Beijing PET Technology Co., Ltd, China), and a PET/CT scanner (Siemens, Germany).

Synthesis and characterization of ^{19}F-MLN-4760 and ^{18}F-MLN-4760

Cold labeling experiments were first performed for the exploration of optimal reaction conditions. To avoid the occurrence of side reactions such as hydrolysis of fluorine, MLN-4760 was dissolved in a nonprotonic polar solution dimethyl sulfoxide, and KF solution was used to provide F ions. The phase reaction catalyst tetramethylammonium chloride was added at a ratio of 1:20, and the reaction temperature was mainly adjusted and optimized in consideration of the half-life of ^{18}F and the boiling point of dimethyl sulfoxide. The above solutions were sealed in an autoclave and reacted at 140 and 180 °C for 1 h. At the end of the reaction, the products were cooled to room temperature and subjected to LC-MS (A: H_2O–0.05% formic acid, B: 0.05% CH_3CN, 5–5–95–95–5–5% B [0–0.2–1.3–2.5–2.6–3 min], 0.6 mL/min), and the MS was performed using ion positive mode to scan over the range of 50 to 1000 m/z. The reaction temperature (180 °C) at which the cold labeled reaction process was more complete and of higher purity was used as the reaction temperature for ^{18}F labeling.

Cyclotron-produced ^{18}F nuclides were purified by SepPak QMA columns to remove metal ions that may be present. The ^{18}F ions on the QMA column were eluted with saline and recovered. The purified ^{18}F was first heated for 0.5–1 h to zeotropically remove water. Referring to the cold labeling experiments, the phase reaction catalyst tetramethylammonium chloride was added at a ratio of 1:20, and the reaction was sealed in an autoclave at 180 °C for 1 h (Scheme 1). After the reaction, the product was cooled down to room temperature and purified on a sep-pak C-18 column. The total DMSO volume of the reaction system was 1 mL and the activation column was rinsed with 1 mL of pure alcohol followed by 1 mL of pure water. ^{18}F-MLN-4760 was obtained by column adsorption and elution with a 30–50% ethanol–saline solution. The radiochemical purity (RCP)

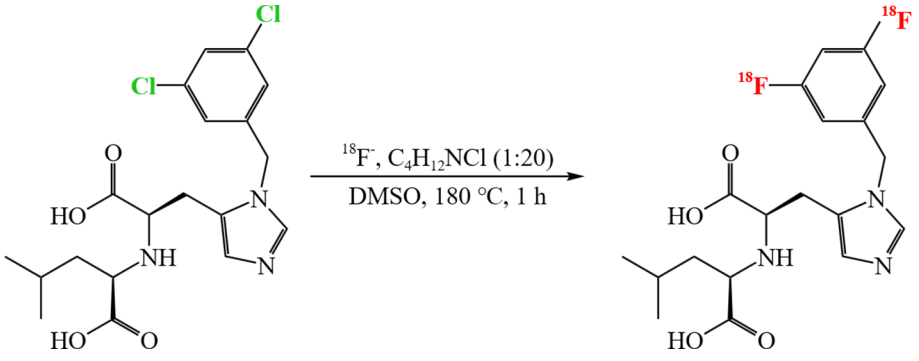

Scheme 1 Radiosynthesis of 18F-MLN-4760, and the colored sites pointed out the site where ^{18}F/Cl exchange takes place partially

was evaluated by HPLC method (Agilent C18 (5 μm, 4.6*250 mm), A: 0.1% TFA-H_2O, B: CH_3CN, 0–50% A [0–10 min], 1 mL/min).

Animal model

All experiments were approved by the Committee on the Science and Technology Ethics Committee of Shanghai University (Institutional Animal Care and Use Protocol number ECSHU-2021-198), and all methods were carried out in accordance with relevant guidelines and regulations. The reporting in this manuscript adhered to the recommendations in the ARRIVE guidelines.

For in vivo studies, 6-week-old humanized ACE2 male mice model (C57BL/6Smoc-$Ace2^{em3(hACE2-flag-Wpre-pA)Smoc}$, Cat. NO. NM-HU-200218) were obtained from Shanghai Model Organisms Center, Inc. The mice were kept in individually ventilated cages under standard conditions with food and water provided ad libitum. Housing conditions were as following: dark/light cycle 12/12 h, ambient temperature around 21–22 ℃ and humidity between 40 and 70%.

PET/CT imaging

A total 5 humanized ACE2 mice were scanned as exemplary cases for in vivo PET/CT imaging. Under 1.5% isoflurane anesthesia, ^{18}F-MLN-4760 (37 MBq/kg) injection and whole-body imaging was performed at 30, 60 and 120 min after injection with PET/CT scanner (Biograph64, Siemens). For the block experiment, 100-fold MLN-4760 was pre-injected and mice were scanned at 30 min post injection (P.I.) of ^{18}F-MLN-4760. The mice were placed in a prone position with the head fixed forward in the central area of PET/CT device and signal acquisition were acquired for 3 min, and CT images were acquired for 1 min (tube voltage: 120 kVp; tube current: 35 mA; average frame: 1.0; fliter thickness: 1 mm). The postprocessing workstation TureD system was utilized for image reconstruction to form maximum intensity projection images. PET/CT workstation provided a quantification value of ^{18}F-MLN-4760 uptake as mean standardized uptake value (SUV_{mean}). The uptake was quantified by drawing regions of interests (ROIs), including heart, lungs, liver, and kidney.

In vivo biodistribution studies

Humanized ACE2 mice were injected in the lateral tail vein with ^{18}F-MLN-4760 (n=3/group, 3.7 MBq/kg) under 1.5% isoflurane anesthesia, and sacrificed by cervical dislocation 30 min later. The mice were kept under persistent anesthesia and warm throughout the injection period. Organs were collected and weighed. Activity content was assessed by γ-counter. Tissue counts and injected dose for the individual mice were decay-corrected to the time of euthanasia. Tissue uptake was expressed as the percentage injected dose per gram of tissue (% injected dose/gram tissue, %ID/g).

Immunohistochemistry

Major organs were analyzed by immunohistochemistry (IHC) using anti-ACE2 antibodies following a standard protocol after biodistribution was completed. The major organs were fixed in 4% paraformaldehyde, and paraffin-embedded tissues were sectioned (4 μm) and deparaffinized. The tissue sections were dewaxed, hydrated, and placed in an antigen-repair solution (0.01 mM sodium citrate buffer) at 60 ℃ overnight. The blocking

solution was discarded, and anti-ACE2 antibody diluted in the appropriate proportion was added onto the sections at 4 ℃ overnight. The configured secondary antibody was dropped onto the tissue sections and incubated at room temperature for 1 h. The reaction was carried out with DAB as a chromogen. Finally, the sections were counterstained with hematoxylin. The IHC images were observed by inverted fluorescence microscope, and the data were processed by Image-Pro Plus software (Version 6.0.0.260, Media Cybernetics Corporation, USA).

Data analysis and statistics

Linear regressions were performed between the average optical density (AOD, AOD = Integrated optical density/Area) and organ uptake (%ID/g) of ^{18}F-MLN-4760. All statistical analyses were performed using SPSS 23.0 software (SPSS Inc.), and graphs were plotted using OriginPro 2019b (OriginLab Inc.). Quantitative data are expressed as the mean ± standard deviation (SD).

Results

Radiochemistry

The reaction conditions of ^{18}F-labeled MLN-4760 were optimized by "cold" labeling experiments, which realized an appreciate ^{18}F/Cl exchange efficiency in lower reaction temperature (180 ℃) and shorter reaction time for the SNAr reaction when comparing with the commonly used halogen-^{18}F exchange reactions (220 ℃) (The mass was verified by LC-MS of the cold labeled product, in which both chlorines were simultaneously substituted for fluorine (Scheme 1). The reaction temperature of 140 ℃ showed additional feedstock peaks and a peak at 1.33–1.34 min in the liquid phase (Fig. 1A), with the maximum mass-to-charge ratio peak at 368.2 being the target molecular ion peak and 339.2 being the molecular ion peak after the loss of ethyl group, which was not yet fully reacted. The results at 180 ℃ showed that the peak at 1.35 min in the liquid phase was the product peak (Fig. 1B). From the mass spectrometry results of ^{19}F-MLN-4760 shown in Fig. 1B, it can find that the mass spectrum at 367.3 is the peak after the removal of one methyl group by ionization of ^{19}F-substituted MLN-4760, and the mass spectrum at 339.3 is the peak after the removal of all branched-chain methyl groups by ionization, at which time the benzene ring was not completely reacted. At this time, both chlorine atoms on the benzene ring were replaced by fluorine.

The reaction condition of ^{18}F-labeled MLN-4760 was carried out at 180 ℃ for 1 h. After labeling with the radionuclide F-18 instead of F-19, the labeled system was purified by a C18 column to remove the catalyst and free $^{18}F^-$. The radiometric purity was of 29.89%, and the yield was about 30% based on radioactivity dose measurements before and after C18 column purification. The UV peak (Fig. 1C) was seen at 1.799 min in agreement with the radioactive peak (Fig. 1D) at the similar retention time. In the following animal experimental, the specific activity of injection was 3.7×10^3 MBq/μmol.

PET/CT imaging

The potential of ^{18}F-MLN-4760 as a PET/CT probe for targeted ACE2 molecular imaging was investigated using a humanized ACE2 mouse model (Fig. 2A). After injecting the prepared ^{18}F-MLN-4760 PET probe into the humanized ACE2 mice for PET/CT imaging, the molecular imaging results (Fig. 2) showed the mice with radiotracer

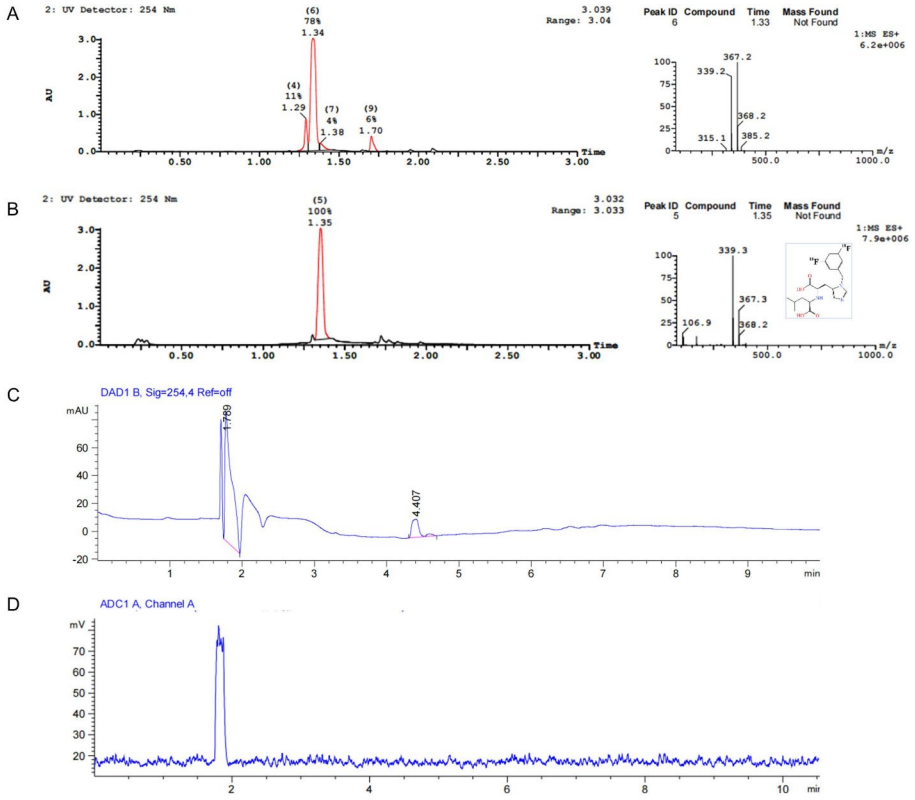

Fig. 1 LC-MS profile and purification of ^{19}F-MLN-4760 at reaction temperatures of (**A**) 140 °C, and (**B**) 180 °C. HPLC profile of (**C**) ^{19}F-MLN-4760 (UV peak) and (**D**) ^{18}F-MLN-4760 (radioactive peak)

accumulation in their heart, lungs, and kidneys, preliminarily demonstrating that ^{18}F-MLN-4760 had a distribution of ACE2 specificity in the humanized ACE2 mice. ^{18}F-MLN-4760 in vivo distribution was rapid, reaching the target in 30 min, and the nonspecifically bound tracer was almost cleared in 120 min, providing a good background for visualization. In addition, the temporal uptake curves of ^{18}F-MLN-4760 indicated that ^{18}F-MLN-4760 had good stability in vivo, with high uptake in major organs even at 120 min after injection (Fig. 2B). The slow distribution of the tracer due to the high presence of ACE2 in the serum may have resulted in a small increase in SUV_{mean} values at 120 min compared with 60 min, with the overall uptake trend remaining unchanged and stabilizing at 30 min. Considering the half-life of ^{18}F, 30 min after injection can be initially designated as the scanning point for ^{18}F-MLN-4760 PET imaging and biodistribution.

The high ACE2–expressing organs and tissues as well as contrast agent–metabolizing organs showed high uptake of ^{18}F-MLN-4760, which fully demonstrated that MLN-4760 continued to have a strong targeting effect on ACE2 after ^{18}F-labeling. Furthermore, these organs with high tracer uptake can be effectively blocked with a pre-injection of 100-fold MLN-4760 (Fig. 2C, 30 min P.I.). The absence of bone deposition in animals at all time points of PET/CT imaging demonstrated that the ^{18}F-labelled drug had good stability in vivo.

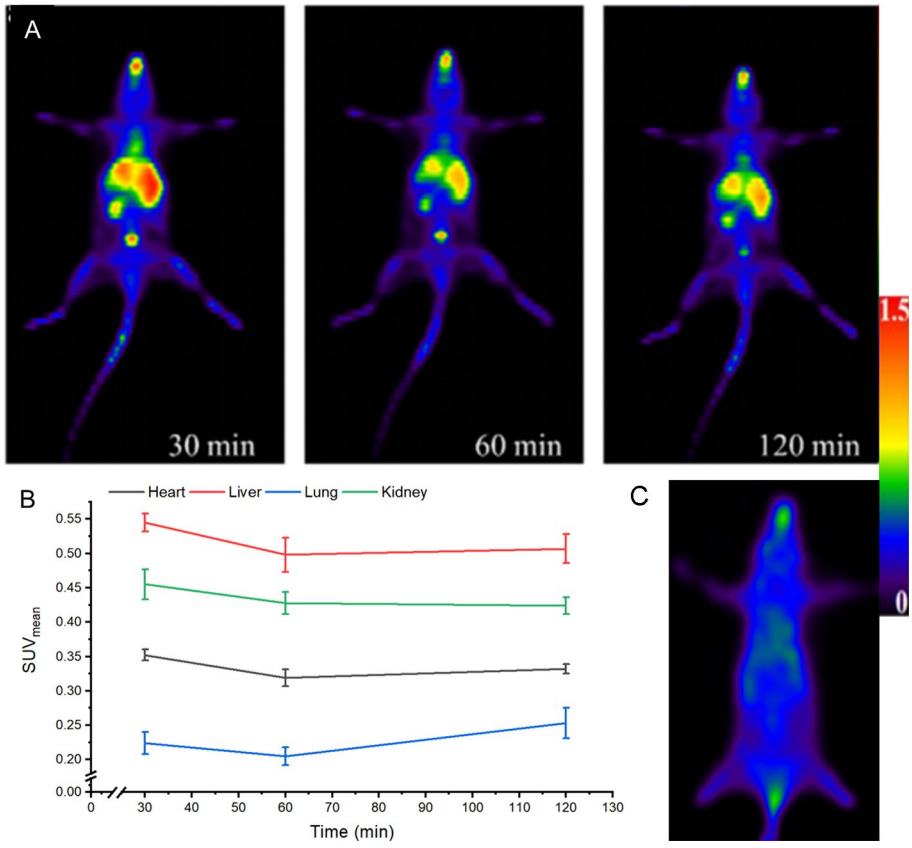

Fig. 2 (**A**) In vivo ^{18}F-MLN-4760 of a humanized ACE2 mouse model. Whole-body scans at 30, 60, and 120 min after injection of ^{18}F-MLN-4760 are shown, with clearly visible high accumulation in ACE2-expressing organs and tissues as well as contrast agent–metabolizing organs, low uptake in other normal organs, and targeting completed at 30 min and nonspecifically bound tracer almost cleared at 120 min. (**B**) Temporal uptake curves of ^{18}F-MLN-4760 (SUV_{mean}) by major organs (heart, lungs, liver, and kidneys) in humanized ACE2 mice over 120 min. (**C**) ^{18}F-MLN-4760 PET of a humanized ACE2 mouse that was pre-injected with 100-fold MLN-4760 and scanned at 30 min P.I

Table 1 In vivo evaluation of biodistribution of ^{18}F-MLN–4760 in humanized ACE2 mice model in 30 min. (%ID/g, mean ± SD)

Organ	humanized ACE2 mice (%ID/g)	Organ	humanized ACE2 mice (%ID/g)
Cerebrum	3.18 ± 4.31	Kidneys	4.73 ± 0.58
Cerebellum	0.40 ± 0.22	Stomach	3.34 ± 2.71
Eyeball	2.84 ± 0.74	Small intestine	2.74 ± 0.90
Parotid	1.93 ± 0.79	Large intestine	3.34 ± 1.88
Oesophagus	11.32 ± 4.13	Testicles	2.91 ± 1.95
Heart	3.26 ± 0.28	Shoulder fat	2.84 ± 1.56
Liver	2.31 ± 0.77	Belly fat	0.48 ± 0.45
Spleen	1.58 ± 2.11	Muscle	2.27 ± 0.75
Lung	2.49 ± 1.09	Medulla	1.83 ± 0.27

n = 3, if not indicated otherwise

p-values are given for comparison of humanized ACE2 mice for each tissue

Biodistribution

In vivo biodistribution data showed that the uptake of ^{18}F-MLN-4760 in the organs and tissues with high ACE2 expression was highly ACE2-specific (Table 1; Fig. 3A). Biodistribution results showed that the uptake of ^{18}F-MLN-4760 by major organs of humanized ACE2 mice remained high at 30 min, and that ^{18}F-MLN-4760 had good specificity and

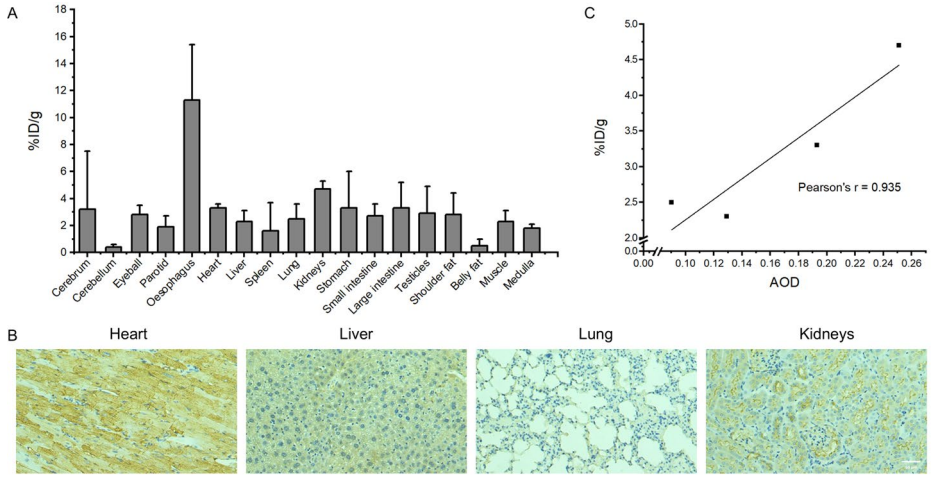

Fig. 3 (**A**) Biodistribution of ^{18}F-MLN-4760 in a humanized ACE2 mouse model. Data were obtained 30 min after ^{18}F-MLN-4760 injection. Values are expressed as %ID/g for organs and tissues. Values are shown as mean ± SD; $n = 3$. (**B**) Immunohistochemical staining of major organs (magnification ×200; scale bar: 50 μm). (**C**) Correlation between tissue uptake (%ID/g) and ACE2 immunohistochemical expression in the humanized ACE2 mouse model (heart, liver, lungs, and kidneys)

in vivo stability in the target binding of ACE2. Among the major organs, the kidneys and heart showed the highest uptake (4.73 ± 0.58%ID/g and 3.26 ± 0.28%ID/g, respectively, at 30 min after injection), whereas the other organs showed very low accumulation and rapid elimination of radiotracer (Fig. 3A).

The same results of ACE2 expression and biodistribution in major organs (heart, liver, lungs, and kidneys) were confirmed by IHC assay for ACE2 (Fig. 3B). Here, the quantitative value of biodistribution in the major organs against ^{18}F-MLN-4760 positively correlated with ACE2 IHC expression ($r = 0.935$, Fig. 3C). This correlation further validated the specificity of ^{18}F-MLN-4760 for ACE2 expression in humanized ACE2 mice.

Discussion

In this study, ^{18}F-MLN-4760—a molecular PET probe targeting ACE2—was successfully synthesized based on the known ACE2 inhibitor MLN-4760. Based on the characteristics of molecular imaging and whole-body scanning, PET imaging using radiotracer can achieve in vivo tracing of the target, which can in turn reveal its functional status and the pathophysiological process of the disease (Rong et al. 2023; Sheng 2015). PET molecular imaging techniques targeting ACE2 have been preliminarily validated as an excellent means to visualize and quantify ACE2 at the in vivo level (Li et al. 2022, 2023a, b). In the design of the precursor, MLN-4760 specifically targets ACE2, but does not cross-react with ACE or other analogues (Joshi et al. 2016). In a previous study, MLN-4760 was developed as a specific ACE2 inhibitor (Dales et al. 2002) and was further proposed as a probe for enzymatic detection of anti-ACE2 neutralizing antibodies (Liao et al. 2013), meeting the biosafety and biospecificity requirements for the development of ACE2 tracers. For example, the associated pathological changes caused by neocoronas are different from the binding domain of ACE2 protein and the receptor-binding domain of Spike protein, so that the binding of ACE2 protein to coronaviruses does not block the uptake of the tracer, i.e., ^{18}F-MLN-4760–based ACE2 PET directly correlates with the apparent ACE2 on the surface of the host cell.

Our previous study of a Ga-68–labeled ACE2 PET tracer (^{68}Ga-cyc-DX600) has been published elsewhere. Compared with ^{68}Ga (Ren et al. 2023; Niedermoser et al. 2015; Beyer et al. 2021), ^{18}F has a small atomic radius, a half-life of 109.8 min, a maximum positron energy of 0.64 MeV, an average range of 0.22 mm in tissues, and excellent nuclear and chemical properties, making it another preferred nuclide for labeling ligands such as peptides. The clinical translational value of a longer-half-life ACE2 tracer may be even higher due to the presence of ACE2 in serum (Ren et al. 2023). The halogen exchange fluorination reaction is a SN_2 nucleophilic substitution reaction, and from the C–X bond energies (C–F: 432 kJ/mol; C–Cl: 339 kJ/mol; C–Br: 209 kJ/mol), it can be seen that the C–F bond energy is the largest, which indicates that it is the most stable, while the bond energies of C–Br and C–Cl are small, and Br and Cl can be used as the leaving groups. However, simple chlorobenzene has difficulty in exchange reaction with F^- even under limiting conditions because the reaction is kinetically controlled. The introduction of an electron-withdrawing group on the aryl ring reduces the electron cloud density of carbon atoms in the 2, 4, 6-positions due to its inducing and conjugating effects, making them susceptible to attack by F^-, which leads to a lower activation energy. Compared with other C-X bonds, fluorine has a stronger electron-withdrawing capacity, which can stabilise the aryl-negative intermediates formed during aromatic nucleophilic substitution, making the reaction easier to carry out. In the present study, the synthetic route is a one-pot procedure, which is a relatively mild process compared with the traditional halogen-^{18}F exchange reactions. The simple and rapid synthetic route does not require multistep synthesis, but the separation of catalyst and purification are necessary. Due to the heavy difference of molar quantity between ^{18}F- and Cl, a mixture of mono-fluorination and no-fluorination was the raw formation of ^{18}F/Cl-exchanged MLN-4760. However, the current procedure was not enough to eliminate the precursor molecule, so, the product was the mixture of ^{18}F-MLN-4760 and MLN-4760. In future research, a try on the totally separation of the cold precursor from ^{18}F-MLN-4760 is needed, so as to increase the specific activity.

Due to the convenience to detect the ^{18}F-MLN-4760 distribution in vivo, ^{18}F-MLN-4760 has the potential to be an ACE2-targeting PET imaging agent. The results of the strain validation data of humanized ACE2 mice showed that the expression of human ACE2 was almost undetectable in wild-type mice, whereas significant expression of human ACE2 could be detected in the lungs, kidneys, and small intestines of ACE2-humanized heterozygous and pure heterozygous mice (Li et al. 2023a, b). In this study, ^{18}F-MLN-4760 validated on the above humanized ACE2 mouse model showed good specificity and in vivo stability in target binding to organismal ACE2 (Fig. 2A), which was basically consistent with the tissues of humanized ACE2 mice with high expression detected by biodistribution. This result fully demonstrated the potential of ^{18}F-labeled MLN-4760 to visualize and quantitatively monitor ACE2 at the in vivo level.

Conclusion

ACE2 is an important physiological and pathological regulatory protein and important biomarker. The ACE2 PET molecular probe ^{18}F-MLN-4760 was synthesized via a ^{18}F/Cl exchange under phase transfer catalysis, and its radiochemical purity and in vivo labeling and binding stability meet the application requirements of nuclear medicine molecular probes. The establishment of PET imaging technology targeting ACE2 at the in vivo

level provides a molecular imaging platform for noninvasive visualization of organ- and tissue-specific ACE2 expression at the in vivo level, and reveals the ACE2 compensation and regulation patterns of disease development.

Abbreviations

ACE2	Angiotensin-converting enzyme 2
RAS	Renin-angiotensin system
ACE	Angiotensin-converting enzyme
Ang-(1-7)	Angiotensin-(1-7)
SNAr	Nucleophilic aromatic substitution reaction
PET/CT	Positron emission tomography/computedtomography
HPLC	High performance liquid chromatography
LC/MS	Liquid chromatography mass spectrometer
IHC	Immunohistochemistry
SUV_{mean}	Mean standardized uptake value
ROIs	Regions of interests
AOD	Average optical density
%ID/g	% injected dose/gram tissue
RCP	Radiochemical purity

Acknowledgements
Not applicable.

Author contributions
P.Z., X.L. and L.Z. contributed to the study conception and design. Data collection was performed by P.Z., K.N., S.X., Q.L., D.L. Data analysis and interpretation was performed by P.Z., H.Y., Z.L., J.Y. The first draft of the manuscript was written by P.Z. R.L. and S.X., and all authors commented on previous versions of the manuscript. All authors read and approved the final manuscript.

Funding
This work was supported by Construction Project of Shanghai Key Laboratory of Molecular Imaging (18DZ2260400, KFKT-2022-08), and the National Natural Science Foundation of China (Youth Program, 82402423).

Data availability
The authors declare that the data supporting the findings of this study are available within the paper and its Supplementary Information files. Should any raw data files be needed in another format they are available from the corresponding author upon reasonable request.

Declarations

Ethics approval and consent to participate
All experiments were approved by the Committee on the Science and Technology Ethics Committee of Shanghai University (Institutional Animal Care and Use Protocol number ECSHU-2021-198), and all methods were carried out in accordance with relevant guidelines and regulations. The reporting in this manuscript adhered to the recommendations in the ARRIVE guidelines.

Consent for publication
Not applicable.

Competing interests
The authors declare that they have no competing interests.

Received: 30 August 2024 / Accepted: 26 November 2024
Published online: 02 December 2024

References

Beyer L, Gosewisch A, Lindner S, Völter F, Mittlmeier LM, Tiling R, et al. Dosimetry and optimal scan time of [(18)F]SiTATE-PET/CT in patients with neuroendocrine tumours. Eur J Nucl Med Mol Imaging. 2021;48:3571–81. https://doi.org/10.1007/s00259-021-05351-x.

Cole EL, Stewart MN, Littich R, Hoareau R, Scott PJ. Radiosyntheses using fluorine-18: the art and science of late stage fluorination. Curr Top Med Chem. 2014;14:875–900. https://doi.org/10.2174/1568026614666140202205035.

Dales NA, Gould AE, Brown JA, Calderwood EF, Guan B, Minor CA, et al. Substrate-based design of the first class of angiotensin-converting enzyme-related carboxypeptidase (ACE2) inhibitors. J Am Chem Soc. 2002;124:11852–3. https://doi.org/10.1021/ja0277226.

Deng X, Rong J, Wang L, Vasdev N, Zhang L, Josephson L, et al. Chemistry for Positron emission tomography: recent advances in (11) C-, (18) F-, (13) N-, and (15) O-labeling reactions. Angew Chem Int Ed Engl. 2019;58:2580–605. https://doi.org/10.1002/anie.201805501.

Donoghue M, Hsieh F, Baronas E, Godbout K, Gosselin M, Stagliano N, et al. A novel angiotensin-converting enzyme-related carboxypeptidase (ACE2) converts angiotensin I to angiotensin 1–9. Circ Res. 2000;87:E1–9. https://doi.org/10.1161/01.res.87.5.e1.

Fontes MA, Silva LC, Campagnole-Santos MJ, Khosla MC, Guertzenstein PG, Santos RA. Evidence that angiotensin-(1–7) plays a role in the central control of blood pressure at the ventro-lateral medulla acting through specific receptors. Brain Res. 1994;665:175–80. https://doi.org/10.1016/0006-8993(94)91171-1.

Gheblawi M, Wang K, Viveiros A, Nguyen Q, Zhong JC, Turner AJ, et al. Angiotensin-converting enzyme 2: SARS-CoV-2 receptor and regulator of the renin-angiotensin system: celebrating the 20th anniversary of the discovery of ACE2. Circ Res. 2020;126:1456–74. https://doi.org/10.1161/circresaha.120.317015.

Hikmet F, Méar L, Edvinsson Å, Micke P, Uhlén M, Lindskog C. The protein expression profile of ACE2 in human tissues. Mol Syst Biol. 2020;16:e9610. https://doi.org/10.15252/msb.20209610.

Huo Y. Current researches and progress on preparation of ^{18}F labeled positron radiopharmacueticals. J Nucl Radiochem. 2015;37:376–80. https://doi.org/10.7538/hhx.2015.37.05.0376.

Joshi S, Balasubramanian N, Vasam G, Jarajapu YP. Angiotensin converting enzyme versus angiotensin converting enzyme-2 selectivity of MLN-4760 and DX600 in human and murine bone marrow-derived cells. Eur J Pharmacol. 2016;774:25–33. https://doi.org/10.1016/j.ejphar.2016.01.007.

Li D, Xiong L, Pan G, Wang T, Li R, Zhu L, et al. Molecular imaging on ACE2-dependent transocular infection of coronavirus. J Med Virol. 2022;94:4878–89. https://doi.org/10.1002/jmv.27958.

Li R, Xu A, Cheng C, Chen J, Wang M, Luo X, et al. ACE2 PET in healthy and diseased conditions. VIEW. 2023a;20230009. https://doi.org/10.1002/VIW.20230009.

Li X, Yin W, Li A, Li D, Gao X, Wang R, et al. ACE2 PET to reveal the dynamic patterns of ACE2 recovery in an infection model with pseudocorona virus. J Med Virol. 2023b;95:e28470. https://doi.org/10.1002/jmv.28470.

Liao K, Sikkema D, Wang C, Lee TN. Development of an enzymatic assay for the detection of neutralizing antibodies against therapeutic angiotensin-converting enzyme 2 (ACE2). J Immunol Methods. 2013;389:52–60. https://doi.org/10.1016/j.jim.2012.12.010.

Lin H, Geurts F, Hassler L, Batlle D, Mirabito Colafella KM, Denton KM, et al. Kidney angiotensin in cardiovascular disease: formation and drug targeting. Pharmacol Rev. 2022;74:462–505. https://doi.org/10.1124/pharmrev.120.000236.

Niedermoser S, Chin J, Wängler C, Kostikov A, Bernard-Gauthier V, Vogler N, et al. In vivo evaluation of ^{18}F-SiFAlin-Modified TATE: a potential challenge for ^{68}Ga-DOTATATE, the clinical gold standard for somatostatin receptor imaging with PET. J Nucl Med. 2015;56:1100–5. https://doi.org/10.2967/jnumed.114.149583.

Ren F, Jiang H, Shi L, Zhang L, Li X, Lu Q, et al. (68)Ga-cyc-DX600 PET/CT in ACE2-targeted tumor imaging. Eur J Nucl Med Mol Imaging. 2023;50:2056–67. https://doi.org/10.1007/s00259-023-06159-7.

Roca-Ho H, Riera M, Palau V, Pascual J, Soler MJ. Characterization of ACE and ACE2 expression within different organs of the NOD mouse. Int J Mol Sci. 2017;18:563. https://doi.org/10.3390/ijms18030563.

Rong J, Haider A, Jeppesen TE, Josephson L, Liang SH. Radiochemistry for Positron emission tomography. Nat Commun. 2023;14:3257. https://doi.org/10.1038/s41467-023-36377-4.

Sahnoun S, Conen P, Mottaghy FM. The battle on time, money and precision: Da[^{18}F] id vs. [^{68}Ga]liath. Eur J Nucl Med Mol Imaging. 2020;47:2944–6. https://doi.org/10.1007/s00259-020-04961-1.

Santos RAS, Sampaio WO, Alzamora AC, Motta-Santos D, Alenina N, Bader M, et al. The ACE2/angiotensin-(1–7)/mas axis of the renin-angiotensin system: focus on angiotensin-(1–7). Physiol Rev. 2018;98:505–53. https://doi.org/10.1152/physrev.00023.2016.

Sheng L. Important events and new frontiers in field of radiopharmaceutical chemistry. J Nucl Radiochem. 2015;37:355–65. https://doi.org/10.7538/hhx.2015.37.05.0355.

Wang J, Beyer D, Vaccarin C, He Y, Tanriver M, Benoit R, et al. Development of radiofluorinated MLN-4760 derivatives for PET imaging of the SARS-CoV-2 entry receptor ACE2. Eur J Nucl Med Mol Imaging. 2024. https://doi.org/10.1007/s00259-024-06831-6.

Wei H, Zhang C, Du X, Zhang Z. Research progress of biosensors for detection of SARS-CoV-2 variants based on ACE2. Talanta. 2023;251:123813. https://doi.org/10.1016/j.talanta.2022.123813.

Widowati W, Wargasetia TL, Rahardja F, Gunanegara RF, Priyandoko D, Gondokesumo ME, et al. hWJMSCs inhibit inflammation and apoptosis in an ARDS cell model. J Taibah Univ Med Sci. 2023;18:1519–26. https://doi.org/10.1016/j.jtumed.2023.06.007.

Xie F, Su P, Pan T, Zhou X, Li H, Huang H, et al. Engineering extracellular vesicles enriched with palmitoylated ACE2 as COVID-19 therapy. Adv Mater. 2021;33:e2103471. https://doi.org/10.1002/adma.202103471.

Yang W, Li L, Zhang K, Ma K, Xie H, Gong Y, et al. ACE2 correlated with immune infiltration serves as a novel prognostic biomarker in clear cell renal cell carcinoma: implication for COVID-19. Int J Biol Sci. 2021;17:20–31. https://doi.org/10.7150/ijbs.51969.

Publisher's note